

Plantar Tactile Feedback for Biped Balance and Locomotion on Unknown Terrain*

J. Rogelio Guadarrama Olvera[†], Emmanuel Dean Leon[‡],
Florian Bergner[§] and Gordon Cheng[¶]

*Institute for Cognitive Systems,
Technical University of Munich, Arcisstrae 21,
80333 Munich, Germany*
[†]rogelio.guadarrama@tum.de
[‡]dean@tum.de
[§]florian.bergner@tum.de
[¶]gordon@tum.de

Received 28 March 2019
Revised 14 August 2019
Accepted 3 November 2019
Published 15 January 2020

This work introduces a new sensing system for biped robots based on plantar robot skin, which provides not only the resultant forces applied on the ankles but a precise shape of the pressure distribution in the sole together with other extra sensing modalities (temperature, pre-touch and acceleration). The information provided by the plantar robot skin can be used to compute the center of pressure and the ground reaction forces. This information also enables the online construction of the supporting polygon and its preemptive shape before foot landing using the proximity sensors in the robot skin. Two experiments were designed to show the advantages of this new sensing technology for improving balance and walking controllers for biped robots over unknown terrain.

Keywords: Tactile feedback; walking; balance; bipedal locomotion.

1. Introduction

Humanoid robot's biped balance and locomotion is a challenging task due to the naturally unstable dynamics of floating base systems. Its difficulty increases, even more, when the terrain is not flat and is unstructured. In such conditions, walking controllers must be adapted to the terrain either by mapping the terrain to plan a set of footholds²⁻⁴ or by reacting compliantly to the terrain modifying the footholds online.⁵⁻⁹

*An earlier version of this paper was presented at the 2018 IEEE-RAS 18th International Conference on Humanoid Robots.¹

[†]Corresponding author.

This is an Open Access article published by World Scientific Publishing Company. It is distributed under the terms of the Creative Commons Attribution 4.0 (CC BY) License which permits use, distribution and reproduction in any medium, provided the original work is properly cited.

Different methods have been developed for mapping the terrain looking for suitable footholds by using cameras,² laser scanners³ or exploratory motions.⁴ Following the reactive approach, different methods have been proposed by including Force-Torque (FT) sensors in the ankles or the joints^{5-7,10,11} or even with contact switches mounted on the sole.^{8,9}

In this paper, a biologically-motivated approach for terrain sensing is presented by mounting robot skin¹²⁻¹⁴ on the foot soles without modifications on the foot architecture. The plantar robot skin can be used to estimate all the states that are required for balance and locomotion^{15,16} (e.g. Center of Pressure (CoP), Zero Moment Point (ZMP) and Centroidal Moment Pivot (CMP)). Besides, it provides complementary information that ankle FT sensors cannot by exploiting the additional sensing modalities. For example, the spatial distribution of force sensors in the robot skin enables the reconstruction of the footprint's pressure distribution and thus an accurate shape of the supporting polygon. In the following sections, the motivation and details of the plantar skin sensor are presented as well as its capabilities to improve biped balance and locomotion.

2. Related Work

Humanoid robot balance and walking controllers require feedback of the ground reaction forces to guarantee the stability of the posture and the gait. In most cases, this information comes from FT sensors mounted in the ankles of the robot.^{5,6} However, the addition of extra sensors to the robot's feet can improve the performance or help simplify the control laws.

Different sensing technologies have been applied to robot soles to improve the performance and versatility of walking controllers. For example, resistive sensor arrays are mounted on the foot soles of small-size humanoid robots without ankle FT sensors to enable the direct measurement of the CoP.¹⁷⁻²⁰

For bigger robot sizes (closer to human size and weight), resistive sensors are combined within the structural layers of the soles to increase the sensing range and endurance.^{21,22} Likewise, other tactile sensing principles have been applied as the optical measurement of rubber deformation²³ or the high-speed pressure sensor grid²⁴ which can acquire the pressure shape of the foothold at a frequency of 1 kHz.

Furthermore, tactile sensors can be combined with other sensing modalities. The perceptual foot developed in Ref. 25 combines the classical ankle FT sensor architecture with a flexible resistive sensor array and an IMU sensor. With this foot architecture, the ZMP and the supporting polygon are acquired at a rate of 100 Hz.

With the addition of contact or pressure sensors on the sole, walking algorithms have been extended to handle unknown terrain conditions^{8,19,26} without complex compliant mechanic designs²⁷ or fast reactive motions.²⁸ Furthermore, even for point feet robots, the detection of premature contacts on a step trajectory can be used to reset the phase of a Central Pattern Generator (CPG).^{9,29} Wider information about

the contacts with the terrain can be exploited not only for footstep compliance but to learn and classify the terrain conditions.^{20,30} By adding more sensing modalities to the sole, more complex interaction conditions can be detected such as the slipperiness of the foothold.³¹

3. Biological Motivation For Plantar Sensing

The postural equilibrium of a human being results from a complex synergy of sensation and actuation.³² It is a dynamic phenomenon which keeps the center of gravity oscillating over the standing feet by the application of antagonistic reflexes triggered by different stimuli.³³ This balance depends on a complex fusion of visual, vestibular, proprioceptive and exteroceptive feedback. It is known that none of them is essential for the purpose of balance, but the lack of each of these kinds of sensory feedback produces different changes in the posture and the motion patterns during stance balance.³⁴ Between the exteroceptive receptors, the cutaneous receptors of the foot sole play an important role for both balance and locomotion.³⁵

The human foot sole is covered with an endurable layer of glabrous skin that apart of protecting the foot from rough surfaces, provides rich sensorial information about the terrain such as texture, hardness, temperature and pressure distribution on the foothold. The role of its cutaneous receptors in the equilibrium control has been studied for more than a century.³⁶ Studies reveal that subjects with the soles anesthetized by hypothermia show increased posture sway while standing. For example in Ref. 37, the subjects presented larger amplitude oscillations while closing the eyes (Romberg's test³⁸) than subjects with non-anesthetized soles. A similar result was generated in Ref. 39 when body sway was galvanically induced in the vestibular system of healthy subjects with anesthetized soles. Furthermore, the inhibition of the sense of touch in the soles also induces delays on the compensatory stepping reactions with different effects depending on the phase and the direction of the step.⁴⁰

The human sole shows various sensitivity to mechanical stimuli in different regions.³⁵ This is because its mechanoreceptive afferents are connected to distinct nerves to transport the data to the spinal cord⁴¹ and because within the regions connected to one of these nerves the receptor density is not uniform and their pressure thresholds are mismatched.⁴² Furthermore, the sensitivity and thresholds of these afferents change according to the phase of a footstep during walking. For example, sensitivity is increased during single support phase on the swing foot and reduced considerably right after footfall.⁴³

In summary, (1) human equilibrium and locomotion rely significantly on the sense of touch provided by the mechanical afferents located on the feet, (2) these afferents are distributed with different sensitivities and thresholds along the sole, (3) the sensitivity and threshold of the afferents depend on the standing or walking phase with clear differences for supporting and swinging leg, (4) the afferents are connected to three main nerve branches that coordinate different reflexes on muscular groups also depending on the walking phase.

4. Plantar Robot Skin

In recent years, robotic tactile sensing gained attention for both industrial^{44,45} and research-oriented platforms like humanoid robots.^{46,47} Robot skin can provide precise information about external contacts with the environment in other parts of the body than the end effectors. With some exceptions as the ones mentioned in Sec. 2, most of the tactile sensors have been developed to provide high sensitivity at low and middle force ranges.⁴⁸ These technologies have successfully improved human–robot interaction,^{46,49} grasping of complex objects^{50–52} and robot safety in industrial environments.^{45,53} Nevertheless, the application proposed in this work requires a skin technology capable of holding the weight of a full-size biped or humanoid robot while resisting the impacts produced during biped locomotion on unknown terrain.

Full-size humanoid robots are designed to work in human environments and to perform tasks with humans. Their mass can be bigger than 100 kg and consequently, the weight of these robots can vary around 980 N without considering payloads. Also, biped walking consists of a succession of single and double support phases. Therefore, the skin sensor required for this application must be capable of holding around 980 N in the area of a foot and still sense variations in the contact pressure.

Due to the heavy load requirement, the suitable robot skins for full-size humanoid robot soles are the resistive matrix arrays^{21,22,25} and the capacitive force cell.⁵⁴ Some of the skin technologies that have proved capable of resisting high pressure and still sense variations are the Tekscan pressure sensors⁵⁵ with pressures larger than 1 MPa, the flexible ROBOSKIN sensors⁵⁴ under pressures larger than 150 kPa, and the stretchable PsSi tactile sheet³⁰ under pressures larger than 150 kPa. Nevertheless, these tactile sensors only provide the pressure shape, and the geometrical mapping over the robot sole must be obtained manually. Even more, they would require protective layers to prevent damage caused by harsh terrain textures.

The robot skin developed at our lab fulfills the load requirement.¹³ Each skin cell with a surface area of 6.9 cm^2 (Fig. 1) can hold more than 80 kg and still sense variations in the applied force (operating pressure $\approx 80\text{ MPa}$). Additionally, it provides four sensing modalities (force, pre-touch, acceleration and temperature) over a uniform spatial distribution that can cover complex curved surfaces.¹² The complete tactile information can be delivered at a rate up to 250 Hz in large scale areas (covering not only the soles) due to new neuromorphic paradigms, such as the even-driven communication architecture.⁵⁶ The robot skin also provides the position of every cell on the sole⁵⁷ which can be used to reconstruct the pressure shape when the foot is on the ground in real-time.

The skin cells are connected with the neighboring cells conforming a dynamic network where the data packets are sent following optimal communication paths to reduce the latency.⁵⁸ This dynamic network configuration is valuable for the foot-sole application because the skin must reconfigure its communication channels in case of hardware damage. Therefore, if a heavy impact is produced between the terrain and the sole, and a skin cell in the sole is damaged, the network reconfigures itself and

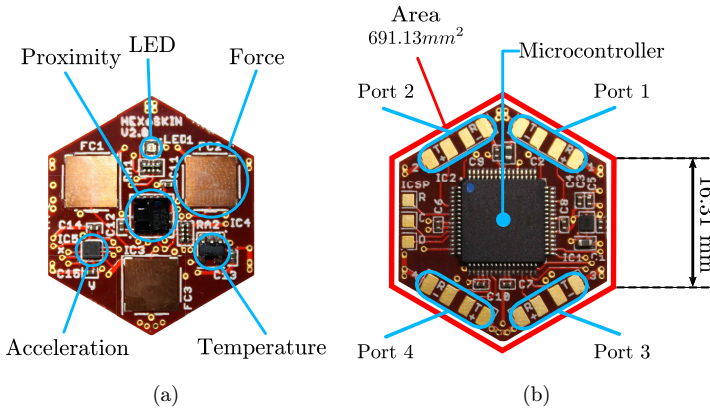


Fig. 1. Robot skin developed at our lab. (a) Each skin cell has four sensing modalities: force \times 3, 3-axis acceleration, temperature and pre-contact (proximity sensor). (b) The data acquisition and network communication are handled by an embedded microcontroller. The cells have four communication ports to connect with the neighboring cells to form a dynamic communication grid.

continues transporting the data generated by the other cells. Nevertheless, the construction of the skin cells is resilient and can hold hard impacts without receiving damage. Additionally, following the biological principle of the sole skin in human feet, the external silicon layer was thickened for this special application to extend its

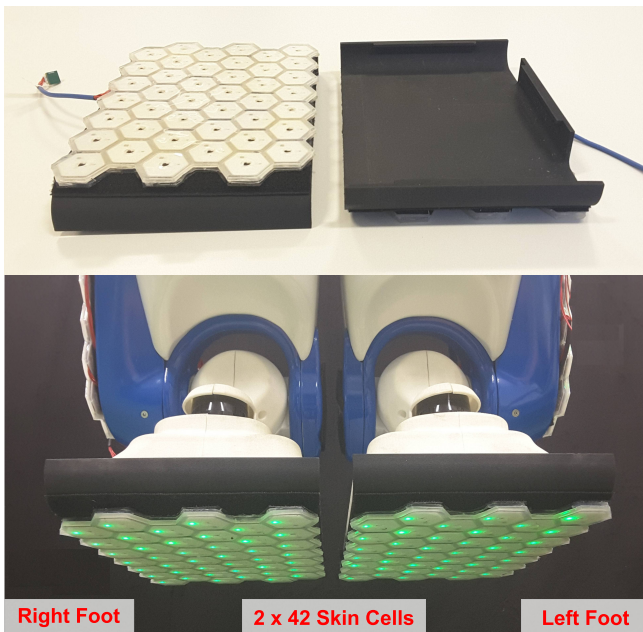


Fig. 2. Skin patches mounted on the soles of the REEM-C robot. Forty two skin cells in each sole, mounted on 3D printed removable sole covers.

lifespan. This silicon material shows a high friction coefficient over different surfaces which improves the stability of the steps, reducing the likelihood of slipping.

Two 42-skin-cell patches were created to cover the soles of our robot as shown in Fig. 2. These patches are mounted on a set of 3D printed removable sole covers which make it easy to mount and dismount without making permanent changes on the robot. This mounting mechanism can be easily adapted to different foot sizes and geometries by creating the mountable covers for the robot foot and the skin patches to cover the sole area.

5. Center of Pressure Estimation

There are different methods to locate the CoP of a robot's foothold with different foot and sensor architectures.⁵⁹ For example, using an array of single-axis force sensors distributed on the sole. The normal force sensors in our robot skin fulfill that requirement. It covers the whole area of the sole with a uniform distribution of normal force sensors as shown in Fig. 2. Then, for a single sole, the position of the CoP is defined as

$$\mathbf{p}_x = \frac{\sum_{j=1}^k p_{jx} F_{jz}}{\sum_{j=1}^k F_{jz}}, \quad \mathbf{p}_y = \frac{\sum_{j=1}^k p_{jy} F_{jz}}{\sum_{j=1}^k F_{jz}}, \quad (1)$$

where, for a group of k skin cells mounted on a robot's sole, F_{jz} is the vertical ground reaction force measured by the j th skin cell located at p_j with respect to the sole coordinate frame O_{sole} as shown in Fig. 3. We denote \mathbf{p} as the computed CoP of the foot sole. Furthermore, the uniform spatial distribution and size of the skin cells enables a fast computation of the contact area by counting the cells that detect contact force over an activation threshold $F_{jz} > \epsilon_F$. All the skin cells that satisfy this condition are called Active Cells. Then, the contact area is

$$A = kA_{cell}, \quad (2)$$

with $A_{cell} \approx 691 \text{ mm}^2$.

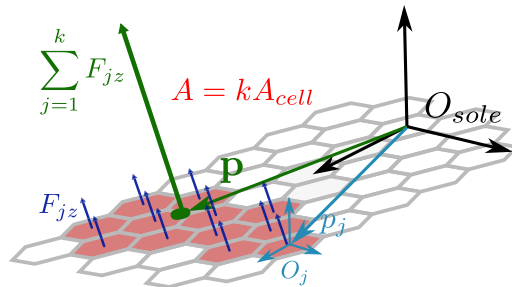


Fig. 3. Computation of the CoP on the sole using the normal force sensors in the robot skin. F_j is the normal force measured by the j th skin cell, p_j its position with respect of the sole coordinate frame and \mathbf{p} is the computed CoP position. As an example of additional information that can be generated with the robot skin, the contact area A is easily computed.

6. Supporting Polygon Acquisition

The extra information the robot skin provides enables the direct acquisition of important balance-stability metrics such as the supporting polygon. As depicted in Fig. 5 the construction of the supporting polygon from skin information starts by finding the active cells [Fig. 5(b)]. Then, for every active cell in the sole, the set of corner points $S_c = [\rho_1 \ \rho_2 \ \dots \ \rho_6]$, $\rho_1 \in \mathbf{R}^4$ (homogeneous points) of the hexagonal skin cell are transformed to the sole frame O_{sole} as shown in Fig. 4 and added to a cluster set [Fig. 5(c)]

$$S_{sole} = \bigcup_{j=1}^k {}^j T_{sole} S_c, \tag{3}$$

where ${}^j T_{sole}$ is the homogeneous transformation from cell frame O_j to the sole frame O_{sole} . Finally, the cluster of contact points on the sole S_{sole} can be used to find the smallest convex hull wrapping S_{sole} using algorithms such as Ref. 60 [Fig. 5(d)]. It is also possible to find concave hulls describing the shape of the ground contact areas with algorithms such as Ref. 61.

For double support, the point clusters of each sole S_{Lsole} and S_{Rsole} can be transformed to world coordinates and concatenated [Fig. 5(f)]

$$S_{feet} = {}^{Lsole} T_{world} S_{Lsole} \parallel {}^{Rsole} T_{world} S_{Rsole}, \tag{4}$$

with ${}^{Lsole} T_{world}$ and ${}^{Rsole} T_{world}$ being the transformation from the left sole frame O_{Lsole} and right sole frame O_{Rsole} to world frame O_{world} , respectively. And then, find the convex hull wrapping S_{feet} which generate the double support supporting polygon [Fig. 5(g)].

This procedure can be applied to other sensing modalities to obtain the temperature footprint of a sole or the pre-touch modality to find a preemptive shape of the supporting polygon from a few centimeters before the foot landing [Fig. 5(e)]. This information is useful to create preemptive controllers for robust walking over unknown terrain.

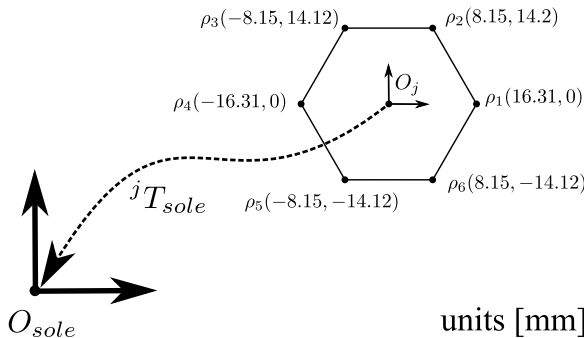


Fig. 4. The corner points of the skin cells are used to populate a cluster which later is used to find the smallest convex hull as supporting polygon.

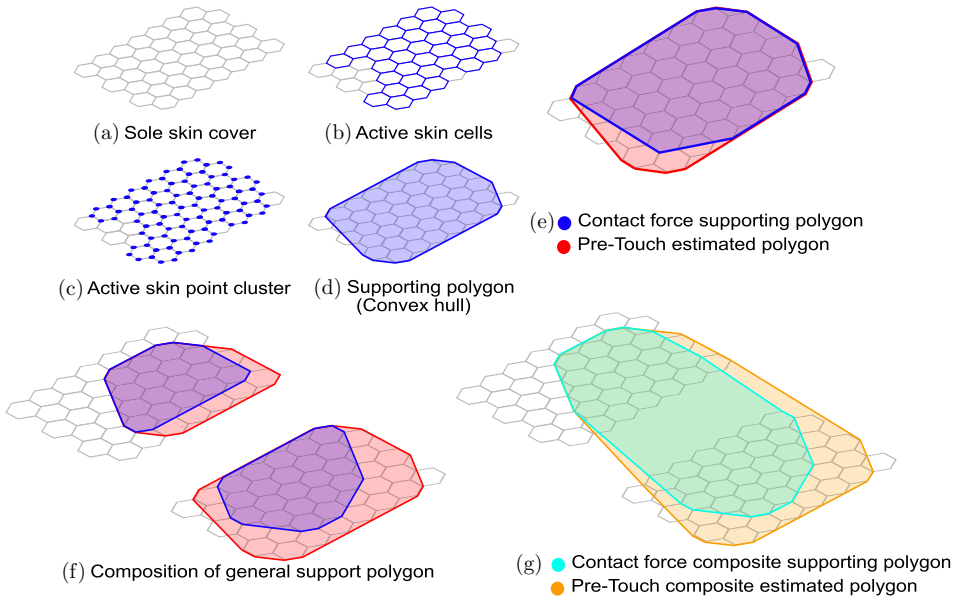


Fig. 5. Supporting polygon acquisition. (a) The spatial distribution of the robot skin over the sole. (b) Detection of active skin cells where $F_{jz} > \epsilon_F$. (c) Active cells point cluster. (d) Convex hull obtained from the point cluster. (e) Two polygons obtained from different sensing modalities: contact force and pre-touch. (f) Polygons of both feet. (g) Composite supporting polygon and pretouch polygon (convex hull from feet polygons).

7. Experimental Results

In this section, the methods described above are experimentally evaluated. The results obtained using robot skin are compared to similar methods using ankle FT sensors. The controllers were implemented on an 86 kg REEM-C humanoid robot with the skin sole covers shown in Fig. 2.

The measurement of the CoP and the reconstruction of the supporting polygon from raw skin data are shown in Fig. 6. First, we identify the active cells as shown in Fig. 6(a). The cells where the pre-touch sensor is active are marked in red and the cells which detect contact force are marked in blue. With the active cells data, as shown in Fig. 6(b), we compute the CoP of each foot with the method described in Sec. 5. With this data, as shown in Fig. 6(c), we also construct the supporting polygon and the pre-touch polygon for each foot using the method described in Sec. 6. Finally, we combine the feet's polygons to construct the composite supporting polygon and the composite pre-touch polygon as described at the end of Sec. 6.

In the following sections, the skin measurements are used to show how tactile feedback can be used in a balance controller and to re-plan steps when an obstacle is detected under the foot during walking.

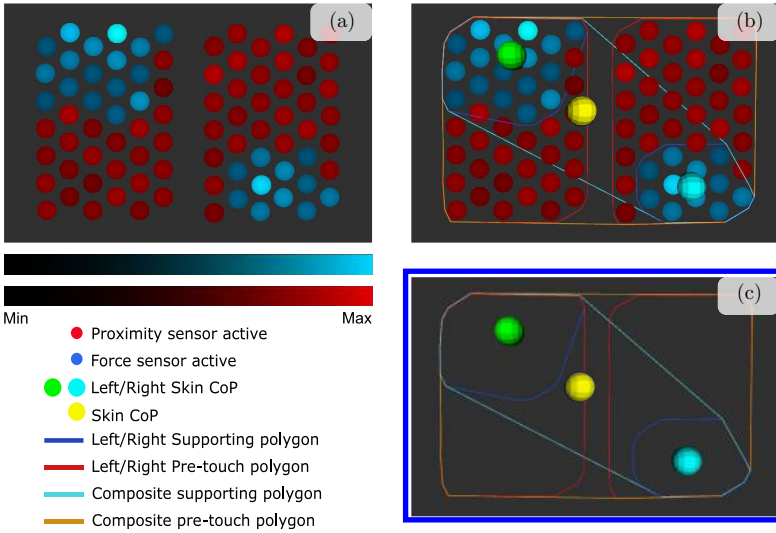


Fig. 6. Snapshots of the sensor data from the robot skin in ROS-Rviz. (a) Raw sensor data from Force sensors and pre-touch sensors. (b) Computation of local and global CoP, supporting polygon and pre-touch polygon. (c) Final representation of the Left and Right CoP, the general CoP, the supporting polygons and pre-touch polygons.

7.1. ZMP in a balance controller

The online acquisition of the CoP can be used to compute the ZMP feedback for stable balance controllers and dynamically balanced walking controllers.¹⁶ To assess the performance of the skin ZMP acquisition, a bench test was implemented comparing the ZMP position estimated by both the robot skin and ankle FT sensors in a balance controller. The feedback law used for this test is the 2D CP-ZMP regulator controller.⁶²

$$\xi = \mathbf{x} + \frac{\dot{\mathbf{x}}}{\omega}, \quad (5)$$

$$\mathbf{p}_d = \xi + \frac{k_\xi}{\omega}(\xi - \xi_d), \quad (6)$$

$$\dot{\mathbf{x}}_d = k_f(\mathbf{p} - \mathbf{p}_d) + k_x(\mathbf{x}_d - \mathbf{x}), \quad (7)$$

where $\omega = \sqrt{\frac{g}{x_z}} \in \mathbf{R}$ is the inverted pendulum frequency at CoM height \mathbf{x}_z , $\mathbf{p} \in \mathbf{R}^2$ and $\mathbf{p}_d \in \mathbf{R}^2$ are the real and desired ZMP, $\xi \in \mathbf{R}^2$ and $\xi_d \in \mathbf{R}^2$ are the real and desired CP, $\mathbf{x} \in \mathbf{R}^2$ and $\mathbf{x}_d \in \mathbf{R}^2$ are the real and desired CoM positions and k_ξ , k_f and k_x are positive gains. The controller was tuned to be compliant to external pushing forces and return to a standing position afterwards. The tuned parameters are listed in Table 1.

The robot was standing on both legs keeping balance and was pushed and pulled by an operator to introduce unknown disturbances on the controller as shown in

Table 1. Balance control parameters.

Parameter	Value
ξ_d	$0 \in \mathbf{R}^2$ [m]
\mathbf{x}_d	$0 \in \mathbf{R}^2$ [m]
\mathbf{x}_z	0.8 [m]
k_ξ	1.5
k_f	0.5
k_x	1.0
ϵ_F	0.15 [kg]

Fig. 7. The plots in Figs. 8(a), 8(e) and 8(c), 8(f) show the estimated ZMP x and y components used directly as feedback in the balance controller (assuming both soles are in full contact with the ground). In these plots, a comparison of the ZMP measured by the FT sensors and the robot skin is presented. The difference in the estimation of the ZMP between the FT sensor and the robot skin $\mathbf{p}_{FT} - \mathbf{p}_{skin}$ is shown in Figs. 8(b), 8(g) and 8(d), 8(h). The plots in Fig. 9 show the comparison of the estimated ZMP with the FT sensors and the skin in the xy plane. Figure 9(a) shows the local ZMP in each foot and the supporting polygon detected for each foot. Figure 9(b) shows the composite ZMP and supporting polygon.

The experiment was conducted two times, first using the skin measured ZMP as feedback in the balance controller and then using the ZMP estimated with the FT sensor. In both cases, the gains of the balance controller were the same. The operator

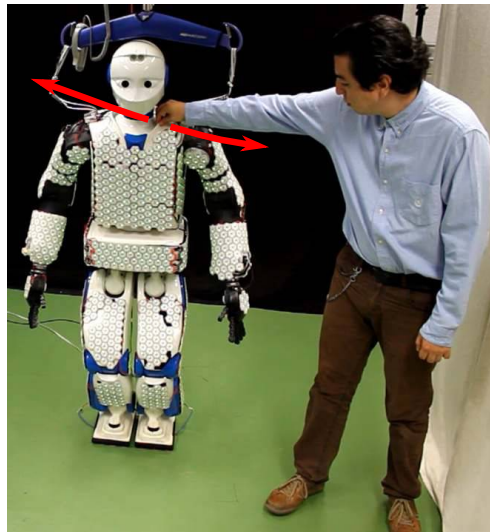


Fig. 7. An experimental test of the ZMP estimation using robot skin. The robot is standing executing a CoM-ZMP compliant balance controller and an operator is pushing the upper body to disturb its balance. The ZMP used in the feedback loop was estimated using the robot skin.

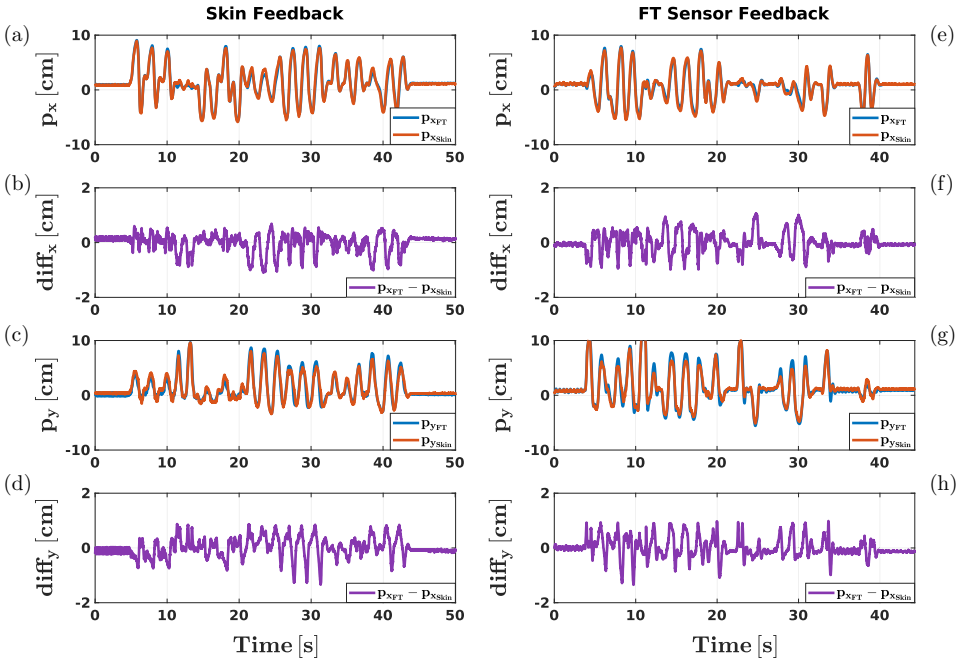
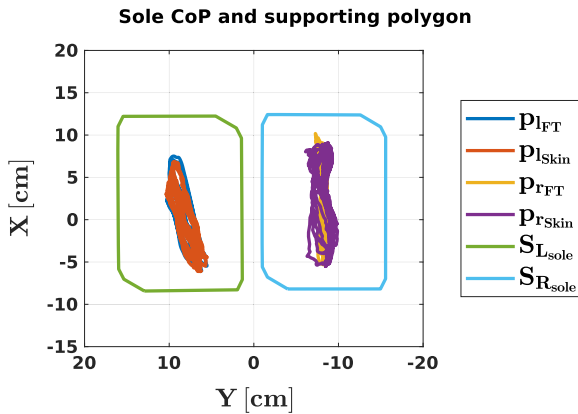
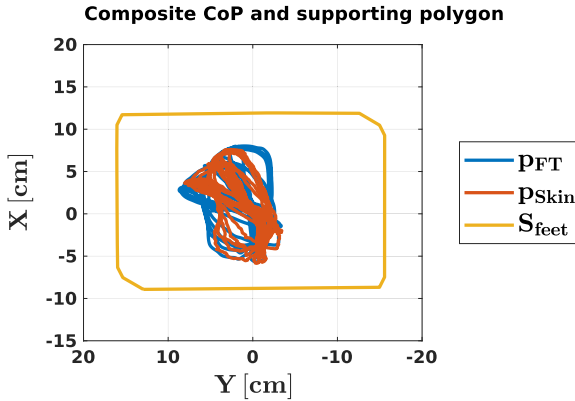


Fig. 8. Data plot of the balance experimental test (Fig. 7). The ZMP was estimated using two different sensors: the robot’s ankle FT sensors (blue), and the robot skin on the sole (red). The experiment was recorded twice, first using the skin ZMP as feedback in the balance controller and then, using the FT sensor ZMP. (a, e) x component of the ZMP. (b, f) difference between the FT sensor and robot skin ZMP x component. (c, g) y component of the ZMP. (d, h) difference between the FT sensor and the robot skin ZMP y component.



(a)

Fig. 9. 2D Data plot of the CoP experimental test shown in Fig. 7. (a) Single sole FT sensor CoP (left p_{FT} and right p_{rFT}), skin CoP (left p_{Skin} and right p_{rSkin}), and supporting polygon (left S_{Lsole} and right S_{Rsole}). (b) Composite FT sensor CoP p_{FT} , skin CoP p_{Skin} and the composite supporting polygon S_{feet} .



(b)

Fig. 9. (Continued)

pushed and pulled the robot from the neck to induce compliant motions in the robot body. When the external force was removed, the robot came back to the desired ZMP position located at the center of the supporting polygon. During the experiment, the ZMP was deviated up to 10 cm from the reference (located at 0 cm) by the external forces. However, it never reached the supporting polygon border to prevent breaking the full-sole contact assumption. The most considerable difference between the ZMP estimation from the FT sensor and the skin was approximately 1 cm and, although the magnitude of the disturbances was unknown, the balancer controller showed a stable behavior in both cases.

7.2. Footstep feasibility check and re-plan

This experiment is designed to examine the advantages the plantar robot skin has over the ankle FT sensors for footstep re-planning over unknown terrain. The robot is intended to walk on a straight line without knowing the geometry of the terrain. The walking controller is designed for flat terrain and does not consider ankle compliance. If an early contact occurs during the swing-leg phase (Fig. 10), the feasibility of stepping on the detected obstacle is evaluated with a simple rule which only uses the information acquired during the impact. If the obstacle is considered as stable, the robot continues walking over it following the planned footsteps. If the obstacle is considered as not safe, the footstep is re-planned to circumvent the obstacle and the robot continues walking as shown in Fig. 11. To check the step feasibility, the following rules are designed with the different sensors:

- (a) **With the FT sensors**, the moment produced at the ankle by the collision M_s (Fig. 10) is compared to a feasibility threshold of ϵ_t . This was defined under the assumption that the impact of a flat foot over flat terrain produces only vertical force. Therefore, if $M_s \geq \epsilon_t$ the step must be re-planned.

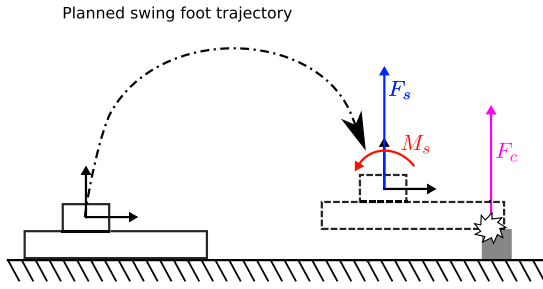


Fig. 10. The trajectory of the swing foot during the experiment. When a premature contact is detected, the forces and moments in the ankle are measured by the FT sensor to evaluate if the obstacle is safe to step on it.

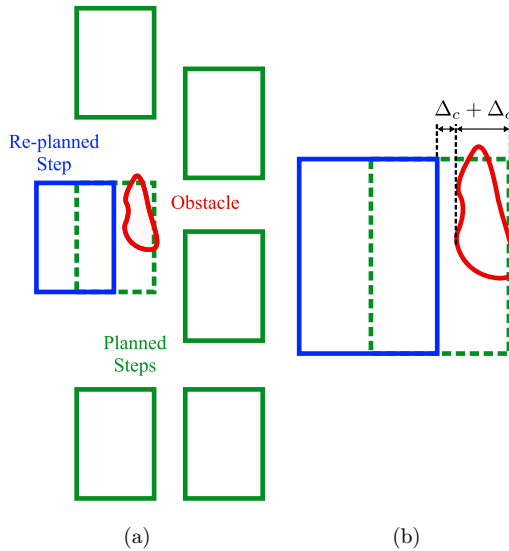


Fig. 11. Walking on unknown terrain experiment. (a) If a foothold is not safe to step onto it, the robot must re-plan to sidestep the detected obstacle. (b) The re-planned step must consider the size of the obstacle Δ_o and a clearance distance Δ_c .

- (b) **With the robot skin**, the relation $\frac{A_p}{A_s}$ is compared to a feasibility threshold of ϵ_A , where A_p is the area of the supporting polygon detected at the moment of the impact, and A_s is the total foot sole area (measured directly from the robot's foot). This rule was designed under the assumption that a safe foothold must cover at least a certain percentage of the sole area to provide enough surface to generate enough friction for stepping on it. Therefore, if $\frac{A_p}{A_s} \leq \epsilon_A$ the step must be re-planned.

Both rules are analogous. However, the FT sensor cannot directly measure the contact area. Thus, it cannot be used for rule *b* while the plantar robot skin can be

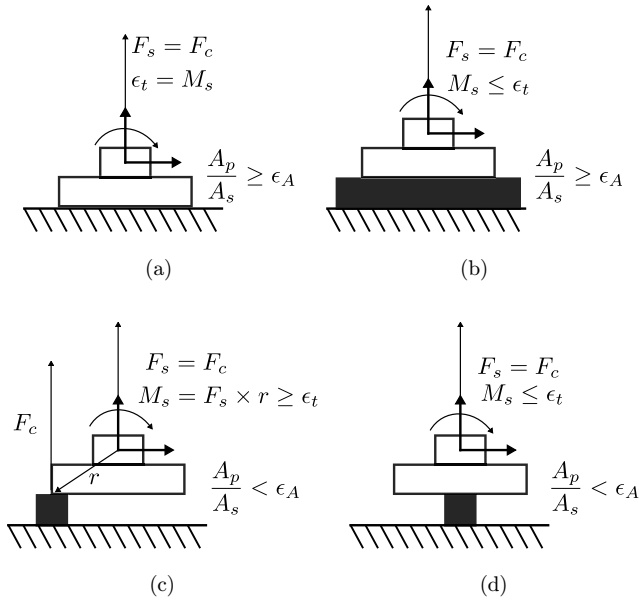


Fig. 12. Different conditions for step feasibility evaluation. (a) With no obstacle, both feasibility rules result in no re-plan. (b) With a big flat obstacle, both feasibility rules result in no re-plan. (c) With a small flat obstacle hit with the border of the sole, both feasibility rules trigger a step re-plan. (d) With a small flat obstacle hit with the center of the sole, just below the FT sensor, the FT sensor rule does not trigger the re-plan, while the robot skin detects the unsafe condition and triggers the re-plan.

used for both. This is one major advantage of having more information about the ground contacts.

The conditions for step re-plan are represented in Fig. 12. For the cases where the contact provides a large flat surface, both rules *a* and *b* result in no re-plan Figs. 12(a) and 12(b). If the contact is produced by a small flat obstacle Fig. 12(c), both rules trigger a step re-plan. All these conditions are correctly evaluated by both, the FT sensors and the robot skin. Nevertheless, when premature contact generates a moment, which is not large enough, the FT sensor fails to detect small surfaces and considers them as similar to a big flat obstacle Fig. 12(b). For example, when a small flat obstacle is touched with the sole right below the FT sensor Fig. 12(d). On the other hand, the robot skin can measure the small obstacle area and trigger a step re-plan.

Right after the first contact, the robot skin can additionally provide the exact distance to sidestep an obstacle. We can obtain the obstacle's width Δ_o from the bounding box of the supporting polygon and the clearance distance Δ_c from the geometry of the foot sole. With this information, we can easily re-plan the step as shown in Fig. 11(b).

Figure 13 shows the experimental comparison for an obstacle with the shape shown in Fig. 12(d). The FT sensor fails to detect the unsafe foothold and the

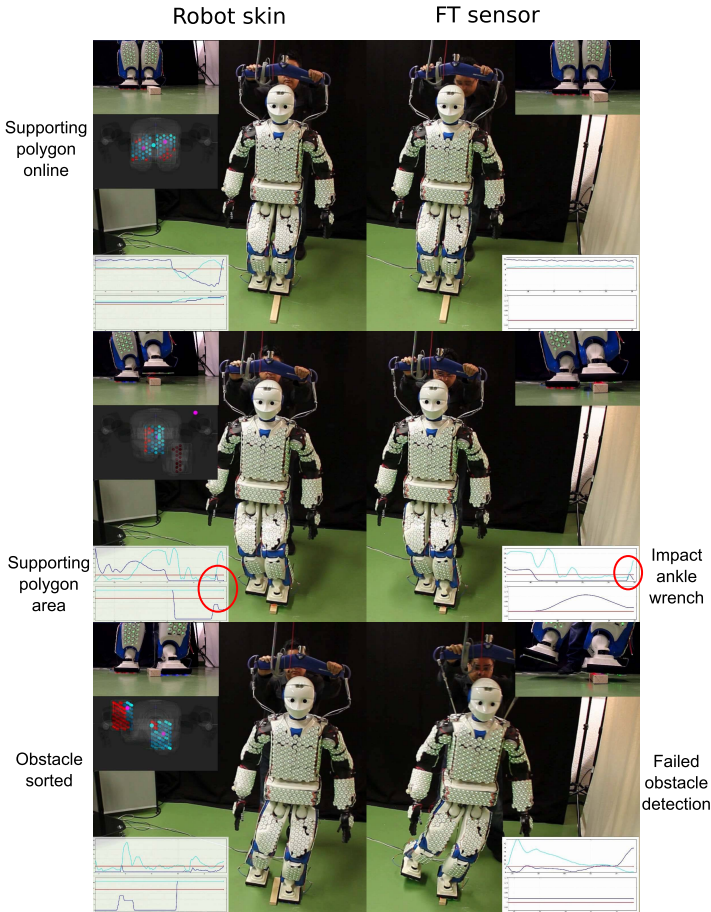

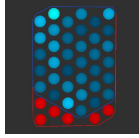

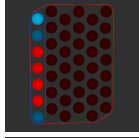

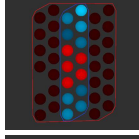
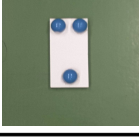
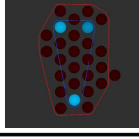


Fig. 13. Experimental evaluation of the step feasibility rules using FT sensors and robot skin. On the left-hand side, the robot skin successfully detects the small area of the obstacle and triggers a step re-plan with the exact distance required to sidestep the obstacle. On the right-hand side, the FT sensor fails to detect the unsafe condition and the walking controller tries to step on the obstacle leading the robot to fall.

walking controller tries to step onto the obstacle causing the robot to fall. The robot skin detects correctly the unsafe obstacle and triggers the step re-plan with the exact distance to sidestep the obstacle and continues walking.

The walking test was performed eight times using four different obstacles as shown in Table 2. For each obstacle, the test was run once using only the FT sensor and once using only the robot skin. The thresholds for the feasibility check rules are ϵ_t for the FT sensor and ϵ_A for the contact area. The FT sensor failed with obstacles 3 and 4 which provide a small flat area that was assumed to be large enough to support the robot. Obstacle 4 is made with 3 small spheres which are providing round surfaces similar to stepping on pebbles. This three-point contact condition is not detectable by the FT sensor without exploratory motions.

Table 2. Tested obstacles. **Green:** Robot completed the test. **Red:** Robot fell down.

No.	Obstacle footprint	M_s [Nm] $\epsilon_t = 8.0$	A_p/A_s $\epsilon_A = 0.8$	Handled by FT-sensor	Handled by Robot skin
1	 	6.5	0.85	Stepping on obstacle	Stepping on obstacle
2	 	8.6	0.16	Footstep re-plan	Footstep re-plan
3	 	6.0	0.33	Stepping on obstacle	Footstep re-plan
4	 	4.5	0.23	Stepping on obstacle	Footstep re-plan

8. Conclusion

The plantar robot skin sensor presented in this work enables the direct measurement of the ground contact forces, together with the spatial information related to them. This plantar sensor can be used to complement ankle sensors in adding redundancy, and combined force perception in a similar manner as human feet.

Plantar tactile sensing proved capable of measuring the ZMP and resultant ground reaction forces similar to ankle FT sensors. These measurements can be used as feedback for balance using the same control techniques as with FT sensors. Additionally, plantar robot skin provides geometrical information from the feet's ground interaction forces. Such information is useful to map the pressure distribution of the footprint, and consequently to construct an accurate shape of the supporting polygon. With this information, balance and walking controllers can adapt online the kinematic constraints to ensure stability without the need for extra exploratory motions or complex constraint estimation methods.

Extra sensing modalities provide information about other terrain conditions or even a preemptive shape of the foothold before foot landing. The spatial resolution of tactile sensors can be used for online step re-planning, as shown in the experimental section. With the extra information about the terrain, it becomes feasible to estimate the size and geometry of small obstacles that can be easily side-stepped instead of walked over.

In future works, we will explore the benefits of exploiting the flexible sensitivity, spatial distribution and additional sensing modalities of the plantar robot skin for developing robust balance and dynamic walking controllers for unknown terrain.

Acknowledgment

Special acknowledgement to the Mexican National Council of Science and Technology (CONACYT) for supporting the first author.

References

1. J. R. Guadarrama-Olvera, F. Bergner, E. Dean and G. Cheng, Enhancing biped locomotion on unknown terrain using tactile feedback, in *2018 IEEE-RAS 18th Int. Conf. Humanoid Robots (Humanoids)* (IEEE, 2018), pp. 1–9.
2. D. Kanoulas, C. Zhou, A. Nguyen, G. Kanoulas, D. G. Caldwell and N. G. Tsagarakis, Vision-based foothold contact reasoning using curved surface patches, in *2017 IEEE-RAS 17th Int. Conf. Humanoid Robotics (Humanoids)* (IEEE, 2017), pp. 121–128.
3. S. Kuindersma, R. Deits, M. Fallon, A. Valenzuela, H. Dai, F. Permenter, T. Koolen, P. Marion and R. Tedrake, Optimization-based locomotion planning, estimation, and control design for the atlas humanoid robot, *Auton. Robots* **40** (2016) 429–455.
4. Y. Lee, H. Lee, S. Hwang and J. Park, Terrain edge detection for biped walking robots using active sensing with vcop-position hybrid control, *Robot. Auton. Syst.* **96** (2017) 41–57.
5. M. Morisawa, S. Kajita, F. Kanehiro, K. Kaneko, K. Miura and K. Yokoi, Balance control based on capture point error compensation for biped walking on uneven terrain, in *2012 12th IEEE-RAS Int. Conf. Humanoid Robots (Humanoids)* (IEEE, 2012), pp. 734–740.
6. J.-Y. Kim, I.-W. Park and J.-H. Oh, Walking control algorithm of biped humanoid robot on uneven and inclined floor, *J. Intell. Robot. Syst.* **48** (2007) 457–484.
7. Z. Li, C. Zhou, N. Tsagarakis and D. Caldwell, Compliance control for stabilizing the humanoid on the changing slope based on terrain inclination estimation, *Autonomous Robots* **40** (2016) 955–971.
8. M. Khadiv, S. A. A. Moosavian, A. Yousefi-Koma, H. Maleki and M. Sadedel, Online adaptation for humanoids walking on uncertain surfaces, *Proc. Ins. Mech. Eng I, J. Syst. Control Eng.* **231** (2017) 245–258.
9. S. Aoi and K. Tsuchiya, Stability analysis of a simple walking model driven by an oscillator with a phase reset using sensory feedback, *IEEE Trans. Robot.* **22** (2006) 391–397.
10. C. Hubicki, J. Grimes, M. Jones, D. Renjewski, A. Spröwitz, A. Abate and J. Hurst, Atrias: Design and validation of a tether-free 3d-capable spring-mass bipedal robot, *Int. J. Robot. Res.* **35** (2016) 1497–1521.
11. K. Van Heerden and A. Kawamura, Biped robot position control with stability-based ground reaction force and velocity constraints, *IEEJ J. Ind. Appl.* **2** (2013) 30–39.
12. P. Mittendorfer and G. Cheng, Humanoid multi-modal tactile sensing modules, *IEEE Trans. Robot.* **27** (2011) 401–410.
13. P. Mittendorfer and G. Cheng, Integrating discrete force cells into multi-modal artificial skin, in *2012 12th IEEE-RAS Int. Conf. Humanoid Robots (Humanoids 2012)* (IEEE, 2012), pp. 847–852.

14. G. Cheng, E. Dean-Leon, F. Bergner, J. R. G. Olvera, Q. Leboutet and P. Mittendorfer, A comprehensive realization of robot skin: Sensors, sensing, control, and applications, *Proc. IEEE* **107** (2019) 2034–2051.
15. M. Vukobratovic and D. Juricic, Contribution to the synthesis of biped gait, *IEEE Trans. Biomed. Eng.* **BME-16**(1) (1969) 1–6.
16. M. Vukobratović and B. Borovac, Zero-moment point thirty five years of its life, *Int. J. Humanoid Robotics* **1** (2004) 157–173.
17. M. Shimojo, T. Araki, A. Ming and M. Ishikawa, A zmp sensor for a biped robot, in *Proc. 2006 IEEE Int. Conf. Robotics and Automation, 2006, ICRA 2006* (IEEE, 2006), pp. 1200–1205.
18. K. Suwanratchatamane, M. Matsumoto and S. Hashimoto, A simple tactile sensing foot for humanoid robot and active ground slope recognition, in *2009 IEEE Int. Conf. Mechatronics* (IEEE, 2009), pp. 1–6.
19. Y.-D. Hong and J.-H. Kim, 3-d command state-based modifiable bipedal walking on uneven terrain, *IEEE/ASME Trans. Mechatronics* **18** (2013) 657–663.
20. M. A. Hoepflinger, C. D. Remy, M. Hutter, L. Spinello and R. Siegwart, Haptic terrain classification for legged robots, in *2010 IEEE Int. Conf. Robotics and Automation (ICRA)* (IEEE, 2010), pp. 2828–2833.
21. G.-i. Kinoshita, T. Kimura and M. Shimojo, Dynamic sensing experiments of reaction force distributions on the sole of a walking humanoid robot, in *Proc. 2003 IEEE/RSJ Int. Conf. Intelligent Robots and Systems (IROS 2003)*(Cat. No. 03CH37453) (IEEE, 2003), Vol. 2, pp. 1413–1418.
22. K. Fondahl, D. Kuehn, F. Beinertsdorf, F. Bernhard, F. Grimminger, M. Schilling, T. Stark and F. Kirchner, An adaptive sensor foot for a bipedal and quadrupedal robot, in *2012 4th IEEE RAS & EMBS Int. Conf. Biomedical Robotics and Biomechanics (BioRob)* (IEEE, 2012), pp. 270–275.
23. V. Chernyak, E. Claretti, S. S. Nestinger and E. Torres-Jara, Caminante: A platform for sensitive walking, in *Nature-Inspired Mobile Robotics* (World Scientific, 2013), pp. 351–358.
24. Y. Takahashi, K. Nishiwaki, S. Kagami, H. Mizoguchi and H. Inoue, High-speed pressure sensor grid for humanoid robot foot, in *2005 IEEE/RSJ Int. Conf. Intelligent Robots and Systems* (IEEE, 2005), pp. 3909–3914.
25. B. Wu, F. Shen, Y. Ren, J. Luo and Z. Wu, Development of an integrated perceptual foot system for humanoid robots, *Int. J. Robot. Autom.* **27** (2012) 217.
26. J. Yi, Q. Zhu, R. Xiong and J. Wu, Walking algorithm of humanoid robot on uneven terrain with terrain estimation, *Int. J. Adv. Robot. Syst.* **13** (2016) 35.
27. D. Torricelli, J. Gonzalez, M. Weckx, R. Jiménez-Fabián, B. Vanderborght, M. Sartori, S. Dosen, D. Farina, D. Lefeber and J. L. Pons, Human-like compliant locomotion: State of the art of robotic implementations, *Bioinspiration Biomimetics* **11** (2016) 051002.
28. G. Wiedebach, S. Bertrand, T. Wu, L. Fiorio, S. McCrory, R. Griffin, F. Nori and J. Pratt, Walking on partial footholds including line contacts with the humanoid robot atlas, in *2016 IEEE-RAS 16th Int. Conf. Humanoid Robots (Humanoids)* (IEEE, 2016), pp. 1312–1319.
29. L. Righetti and A. J. Ijspeert, Pattern generators with sensory feedback for the control of quadruped locomotion, in *IEEE Int. Conf. Robotics and Automation, 2008. ICRA 2008* (IEEE, 2008), pp. 819–824.
30. Q. Yuan and J. Wang, Design and experiment of the nao humanoid robot’s plantar tactile sensor for surface classification, in *2017 4th Int. Conf. Information Science and Control Engineering (ICISCE)* (IEEE, 2017), pp. 931–935.

31. T. Okatani, H. Takahashi, T. Takahata and I. Shimoyama, Evaluation of ground slippery condition during walk of bipedal robot using mems slip sensor, in *2017 IEEE 30th Int. Conf. Micro Electro Mechanical Systems (MEMS)* (IEEE, 2017), pp. 1033–1035.
32. L. M. Nashner, Sensory feedback in human posture control, Ph.D. thesis, Massachusetts Institute of Technology (1970).
33. F. A. Hellebrandt, Standing as a geotropic reflex: The mechanism of the asynchronous rotation of motor units, *Am. J. Physiology-Legacy Content* **121** (1938) 471–474.
34. A. Mahboobin, P. J. Loughlin, M. S. Redfern, S. O. Anderson, C. G. Atkeson and J. K. Hodgins, Sensory adaptation in human balance control: Lessons for biomimetic robotic bipeds, *Neural Netw.* **21** (2008) 621–627.
35. J. T. Inglis, P. M. Kennedy, C. Wells and R. Chua, The role of cutaneous receptors in the foot, in *Sensorimotor Control of Movement and Posture* (Springer, 2002), pp. 111–117.
36. W. Heyd, *Der Tastsinn der Fusssohle als Aequilibrirungsmittel des Körpers beim Stehen* (H. Laupp, 1862).
37. E. Orma, The effects of cooling the feet and closing the eyes on standing equilibrium. different patterns of standing equilibrium in young adult men and women, *Acta Phys. Scand.* **38** (1957) 288–297.
38. J. Rogers, Romberg and his test, *J. Laryngol. Otol.* **94** (1980) 1401–1404.
39. M. Magnusson, H. Enbom, R. Johansson and J. Wiklund, Significance of pressor input from the human feet in lateral postural control: The effect of hypothermia on galvanically induced body-sway, *Acta otolaryngol.* **110** (1990) 321–327.
40. S. D. Perry, W. E. McIlroy and B. E. Maki, The role of plantar cutaneous mechanoreceptors in the control of compensatory stepping reactions evoked by unpredictable, multi-directional perturbation, *Brain Res.* **877** (2000) 401–406.
41. H. Gray, *Anatomy of the Human Body*, Vol. 8 (Lea and Febiger, 1878).
42. M. Trulsson, Mechanoreceptive afferents in the human sural nerve, *Exp. Brain Res.* **137** (2001) 111–116.
43. J. Duysens, A. Tax, S. Nawijn, W. Berger, T. Prokop and E. Altenmüller, Gating of sensation and evoked potentials following foot stimulation during human gait, *Exp. Brain Res.* **105** (1990) 423–431.
44. E. Dean-Leon, K. Ramirez-Amaro, F. Bergner, I. Dianov, P. Lanillos and G. Cheng, Robotic technologies for fast deployment of industrial robot systems, in *IECON 2016 — 42nd Annual Conf. IEEE Industrial Electronics Society* (Florence, Italy, 2016), pp. 6900–6907.
45. A. Muxfeldt, J. N. Haus, J. Cheng and D. Kubus, Exploring tactile surface sensors as a gesture input device for intuitive robot programming, in *2016 IEEE 21st Int. Conf. Emerging Technologies and Factory Automation (ETFA)* (IEEE, 2016), pp. 1–4.
46. F. Nori, S. Traversaro, J. Eljaik, F. Romano, A. Del Prete and D. Pucci, icub whole-body control through force regulation on rigid non-coplanar contacts, *Front. Robot. Artif. Intell.* **2** (2015) 6.
47. C. Bartolozzi, L. Natale, F. Nori and G. Metta, Robots with a sense of touch, *Nature Mater.* **15** (2016) 921.
48. R. S. Dahiya, G. Metta, M. Valle and G. Sandini, Tactile sensing-from humans to humanoids., *IEEE Trans. Robotics* **26** (2010) 1–20.
49. B. D. Argall and A. G. Billard, A survey of tactile human–robot interactions, *Robot. Auton. Syst.* **58** (2010) 1159–1176.
50. Y. Ohmura and Y. Kuniyoshi, Humanoid robot which can lift a 30kg box by whole body contact and tactile feedback, in *2007 IEEE/RSJ Int. Conf. Intelligent Robots and Systems* (IEEE, 2007), pp. 1136–1141.

51. C.-H. King, M. O. Cuijlat, M. L. Franco, C. E. Lewis, E. P. Dutton, W. S. Grundfest and J. W. Bisley, Tactile feedback induces reduced grasping force in robot-assisted surgery, *IEEE Trans. Haptics* **2** (2009) 103–110.
52. K. Hsiao, S. Chitta, M. Ciocarlie and E. G. Jones, Contact-reactive grasping of objects with partial shape information, in *2010 IEEE/RSJ Int. Conf. Intelligent Robots and Systems* (IEEE, 2010), pp. 1228–1235.
53. T. L. Lam, H. W. Yip, H. Qian and Y. Xu, Collision avoidance of industrial robot arms using an invisible sensitive skin, in *2012 IEEE/RSJ Int. Conf. Intelligent Robots and Systems* (IEEE, 2012), pp. 4542–4543.
54. P. Maiolino, M. Maggiali, G. Cannata, G. Metta and L. Natale, A flexible and robust large scale capacitive tactile system for robots, *IEEE Sensors J.* **13** (2013) 3910–3917.
55. K. N. Bachus, A. L. DeMarco, K. T. Judd, D. S. Horwitz and D. S. Brodke, Measuring contact area, force, and pressure for bioengineering applications: Using fuji film and tekscan systems, *Med. Eng. Phys.* **28** (2006) 483–488.
56. F. Bergner, E. Dean-Leon and G. Cheng, Event-based signaling for large-scale artificial robotic skin — realization and performance evaluation, in *IEEE/RSJ Int. Conf. Intelligent Robots and Systems (IROS)* (2016), pp. 4918–4924.
57. P. Mittendorf and G. Cheng, 3d surface reconstruction for robotic body parts with artificial skins, in *2012 IEEE/RSJ Int. Conf. Intelligent Robots and Systems (IROS)* (IEEE, 2012), pp. 4505–4510.
58. C. Bader, F. Bergner and G. Cheng, A robust and efficient dynamic network protocol for a large-scale artificial robotic skin, in *2018 IEEE/RSJ Int. Conf. Intelligent Robots and Systems (IROS)* (IEEE, 2018), pp. 1600–1605.
59. S. Kajita, H. Hirukawa, K. Harada and K. Yokoi, *Introduction to Humanoid Robotics*, Vol. 101 (Springer, 2014).
60. F. P. Preparata and S. J. Hong, Convex hulls of finite sets of points in two and three dimensions, *Commun. ACM* **20** (1977) 87–93.
61. J.-S. Park and S.-J. Oh, A new concave hull algorithm and concaveness measure for n-dimensional datasets, *J. Inf. Sci. Eng.* **28** (2012) 587–600.
62. M. Krause, J. Engelsberger, P.-B. Wieber and C. Ott, Stabilization of the capture point dynamics for bipedal walking based on model predictive control, *IFAC Proc.* **45** (2012) 165–171.



Julio Rogelio Guadarrama Olvera received the B.Sc. degree in Mechatronic Engineering from the National Polytechnic Institute (IPN) in 2011 and the M. Sc. degree in Electrical Engineering from the Center for Research and Advanced Studies (CINVESTAV-IPN) in 2013. He is currently pursuing a Ph.D. in electrical engineering at the Chair for Cognitive Systems in the Technical University of Munich. His research focuses on the development of interaction and locomotion controllers for biped humanoid robots, exploiting several sensing modalities.



Emmanuel Dean Leon received the M.Sc. and Ph.D. degrees in Mechatronics from the Center for Research and Advanced Studies (CINVESTAV-IPN) in 2003 and 2006. Since 2013 he is a senior researcher at the Chair for Cognitive Systems, Technical University of Munich (TUM). His research interests include robotics, low-level control, and physical human–robot interaction/collaboration.



Florian Bergner received the B.Sc. and M.Sc. degrees in Electrical Engineering from the Technical University of Munich (TUM), Munich, Germany, in 2011 and 2014, respectively. Since 2014, he has been working toward the Ph.D. degree in electrical engineering at the Chair for Cognitive Systems, TUM. His research interests include multi-modal tactile sensing, large-scale robot skin, sensor networks, sensor fusion, neuromorphic engineering, and event-driven signaling and processing.



Gordon Cheng holds the Chair for Cognitive Systems since 2010, he is Founder and Director of Institute for Cognitive Systems, Faculty of Electrical and Computer Engineering at Technical University of Munich, Munich/Germany. He is also the coordinator of the CoC for Neuro-Engineering — Center of Competence Neuro-Engineering (2013) in the Department of Electrical and Computer Engineering. Prof. Cheng is speaker of the Elite Master of Science program in Neuroengineering (MSNE) of the Elite Network of Bavaria (2016)

He received a Ph.D. (2001) in Systems Engineering from the Department of Systems Engineering, The Australian National University. Bachelor (1991) and Master (1993) degrees in Computer Science from the University of Wollongong, Australia. He has extensive industrial experiences in consultancy as well as contractual development of large software systems. He was also the Founder/CEO of the company, G.T.I. Computing (1995–2006), a company he founded specialising in networking and transport management systems in Australia.

He has been named IEEE Fellow for “contributions in humanoid robotic systems and neurorobotics”. His research interests include, humanoid robotics, cognitive systems, real-time network robot control, brain machine interfaces, bio-mimetic of human vision, computational neuroscience of vision, action understanding, human–robot interaction, active vision, mobile robot navigation and object-oriented software construction.